



August 2007

# Dynamics of electron-trapping materials under blue light and near infrared exposure: an improved model

Ramin Pashaie

*University of Pennsylvania*, [raminp@seas.upenn.edu](mailto:raminp@seas.upenn.edu)

Nabil H. Farhat

*University of Pennsylvania*, [farhat@seas.upenn.edu](mailto:farhat@seas.upenn.edu)

Follow this and additional works at: [http://repository.upenn.edu/ease\\_papers](http://repository.upenn.edu/ease_papers)

---

## Recommended Citation

Ramin Pashaie and Nabil H. Farhat, "Dynamics of electron-trapping materials under blue light and near infrared exposure: an improved model", . August 2007.

Postprint version. Published in *Journal of the Optical Society of America, B*, Volume 24, Issue 8, August 2007, pages 1927-1941.

This paper was published in *Journal of the Optical Society of America, B* and is made available as an electronic reprint with the permission of OSA. The paper can be found at the following URL on the OSA website: <http://josab.osa.org/abstract.cfm?id=140032>. Systematic or multiple reproduction or distribution to multiple locations via electronic or other means is prohibited and is subject to penalties under law.

This paper is posted at ScholarlyCommons. [http://repository.upenn.edu/ease\\_papers/283](http://repository.upenn.edu/ease_papers/283)

For more information, please contact [repository@pobox.upenn.edu](mailto:repository@pobox.upenn.edu).

---

# Dynamics of electron-trapping materials under blue light and near infrared exposure: an improved model

## **Abstract**

Dynamics of electron-trapping materials (ETMs) is investigated. Based on experimental observations, evolution of the ETM's luminescence is mathematically modeled by a nonlinear differential equation. This improved model can predict dynamics of ETM under blue light and near-infrared (NIR) exposures during charging, discharging, simultaneous illumination, and in the equilibrium state. The equilibrium-state luminescence of ETM is used to realize a highly nonlinear optical device with potential applications in nonlinear optical signal processing.

## **Keywords**

fluorescent and luminescent materials, information processing, optical data processing

## **Comments**

Postprint version. Published in *Journal of the Optical Society of America, B*, Volume 24, Issue 8, August 2007, pages 1927-1941.

This paper was published in *Journal of the Optical Society of America, B* and is made available as an electronic reprint with the permission of OSA. The paper can be found at the following URL on the OSA website: <http://josab.osa.org/abstract.cfm?id=140032>. Systematic or multiple reproduction or distribution to multiple locations via electronic or other means is prohibited and is subject to penalties under law.

# Dynamics of electron-trapping materials under blue light and near-infrared exposure: an improved model

Ramin Pashaie<sup>1,\*</sup> and Nabil H. Farhat<sup>1,2</sup>

<sup>1</sup>Department of Electrical and System Engineering, University of Pennsylvania, 200 South 33rd Street, Philadelphia, Pennsylvania 19104-6391, USA

<sup>2</sup>Institute of Neurological Sciences, University of Pennsylvania, 3450 Hamilton Walk, Philadelphia, Pennsylvania 19104-6074, USA

\*Corresponding author: raminp@seas.upenn.edu

Received January 8, 2007; accepted April 10, 2007;  
posted April 26, 2007 (Doc. ID 78556); published xx xx, xxxx

Dynamics of electron-trapping materials (ETMs) is investigated. Based on experimental observations, evolution of the ETM's luminescence is mathematically modeled by a nonlinear differential equation. This improved model can predict dynamics of ETM under blue light and near-infrared (NIR) exposures during charging, discharging, simultaneous illumination, and in the equilibrium state. The equilibrium-state luminescence of ETM is used to realize a highly nonlinear optical device with potential applications in nonlinear optical signal processing. © 2007 Optical Society of America

OCIS codes: 160.2540, 200.4560, 200.3050.

## 1. INTRODUCTION

Electron-trapping materials (ETMs) are alkaline-earth sulfides doped with rare-earth luminescence centers [1,2]. Such a material possesses versatile optical properties, including high resolution and wavelength diversity, which make it attractive for a variety of technical applications [1,2]. ETM has been employed in the structure of computational machines such as parallel Boolean logic [3], spatial domain match filtering [4], associative memory [5–7], and adaptive learning [8], as well as optical data storage [1,2], infrared sensors, image intensifiers, and medium-wavelength infrared to visible converters [9,10].

The atomic structure and the dynamics of ETM under blue light and near-infrared (NIR) illumination have been known for sometime [11], and a few approximate models for the optical mechanism of ETM have been presented [12,13]. The first-order mathematical model that governs the ETM's dynamics was proposed in 1993 [12]. This model contained several restrictions; namely, it assumed the trapped electron density is far from saturation, and the effect of interaction between blue photons and the trapped electrons is negligible. Furthermore, in this model, electron-trapping efficiency was assumed to be independent of the current level of the trapped electron density. With these simplifications, the charging and discharging processes were modeled by linear and exponential functions, respectively.

A modified version of this early model was presented in 1995 [13] that took into account some of the previously neglected effects. In this modified model, the intensity of the ETM's luminescence was a function of the intensity of both the charging blue light and the discharging NIR exposures. Also, the saturation in the density of trapped electrons was considered in the equations. Both charging

and discharging processes were exponential. Nevertheless, predictions of the model do not agree well with experimental results.

Extending the utility of ETMs to quantitative applications requires a mathematical model that predicts its unique dynamics precisely. In this paper, we present an improved model that can simulate the evolution of ETM's luminescence during charging and discharging, including simultaneous blue light and NIR exposure, and in the equilibrium state. Predictions of the model agree with experimental observations.

In Section 2 we briefly review the physics and the optical mechanism of ETM. The chain of experiments that led us to the improved model are detailed in Section 3, and the mathematical model is presented in Section 4. Section 5 is devoted to the equilibrium-state luminescence of ETM. We show how the equilibrium state of an ETM can be used to conceive nonlinear optical devices. Concluding remarks are given in Section 6.

## 2. DYNAMICS OF ETM UNDER BLUE LIGHT AND NEAR-INFRARED ILLUMINATION

The ETM used in this study is SrS:Eu<sup>2+</sup>,Sm<sup>3+</sup>, which is basically wide-bandgap strontium sulfides (SrS) doped with two types of selected rare-earth elements, Eu<sup>2+</sup> and Sm<sup>3+</sup>. Fabrication of relatively large-area thin films of this ETM is easy. The atomic structure and the optical mechanism of ETM under simultaneous blue light and NIR exposure are depicted in Fig. 1. Both of the two rare-earth doping elements have ground and excited states within the wide bandgap of the host; however, the luminescence centers of Eu<sup>2+</sup> can easily give up an electron to become Eu<sup>3+</sup>, and the electron-trapping centers of the

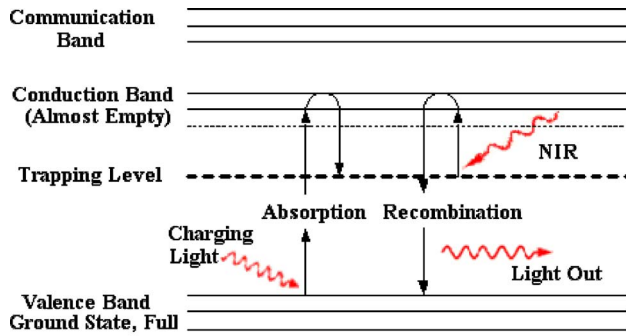
Color:  
Online

Fig. 1. (Color online) Optical mechanism of charging and discharging of ETM. Interaction of blue photons and electrons of the valence band excites the electrons and sends them to the communication band. Those excited electrons will tunnel to the trap level and become trapped electrons. Infrared photons give sufficient energy to the trapped electrons to detrapp and excite them to the communication energy level. These electrons release their extra energy in the form of orange luminescence during their return to the valence band.

<sup>85</sup>  $\text{Sm}^{3+}$  can easily accept an electron to become  $\text{Sm}^{2+}$ . Absorption of blue light with a peak response at  $\approx 450$  nm excites electrons from the ground state to the excited state of  $\text{Eu}^{2+}$  ions. Once in the excited state, electrons tunnel to neighboring  $\text{Sm}^{3+}$  sites and then fall to the ground state to become trapped electrons, leaving behind  $\text{Eu}^{3+}$  and  $\text{Sm}^{2+}$  ions.

<sup>92</sup> Blue photons can also provide sufficient energy to kick the electrons from the trap level to the communication level, where they may interact and return to the ground state accompanied by the emission of photons with peak response at  $\approx 640$  nm (orange light luminescence). However, when the density of trapped electrons is much lower than the density of electrons in the valence band, the probability of interaction between blue photons and electrons of the valence band is higher than having such an interaction with trapped electrons. If blue light illumination persists for a while, a greater number of electrons will be trapped, which increases their chance of interacting with blue photons. As a result, if an ETM with empty trap levels is exposed to blue light illumination, the intensity of the orange light emission will reach the saturation

level after a sharp growth. The intensity of orange light emission during blue light exposure can be used as a means of estimating the density of trapped electrons.

When the blue light is removed, the information carried in by the blue light pattern is stored in the ETM as a trapped electron density distribution. If the charged ETM is exposed to uniform NIR light with peak response at  $\approx 1310$  nm, sufficient energy is provided that the trapped electrons are excited from the ground state of  $\text{Sm}^{2+}$  to the excited state and tunnel back to neighboring  $\text{Eu}^{3+}$  sites. Again, subsequent relaxation from the  $\text{Eu}^{3+}$  excited state to the ground state produces emission of orange light. Under simultaneous illumination of the ETM by constant blue light and NIR exposure, after a transient response, orange emission converges to a constant value that is the equilibrium-state luminescence of the ETM.

Since the mechanism involved is purely electronic, ETMs are fast, possessing nanosecond response times under both blue light and infrared illuminations. They provide long-term storage of information when kept dark and have potential for high-density storage ( $>100$  lp/mm) when fabricated in crystalline thin film form [14].

### 3. EXPERIMENTS

An ordered sequence of experiments has been carried out to verify the dynamics of ETM with the experimental setup illustrated in Fig. 2. A thin layer of electron-trapping material deposited on a  $25\text{ mm} \times 25\text{ mm}$  layer of quartz [15] is exposed to two different sources of light: a bright blue LED and an Exalos 20 mW fiber coupled 1310 nm NIR superluminescence laser diode. A center-hole dark mask is placed on the ETM panel. This mask defines the area of the ETM under illumination in the following experiments. A blue optical filter blocks possible infrared radiation of the blue LED. Drivers of both light sources are precisely controlled by digital-to-analog converters (DACs) of a microcontroller board. An orange optical filter (Semrock LP01-633Rs-25) is placed in front of a cooled avalanche photodiode (APD) module (Hamamatsu CA4777-01) to measure the orange luminescence of the ETM.

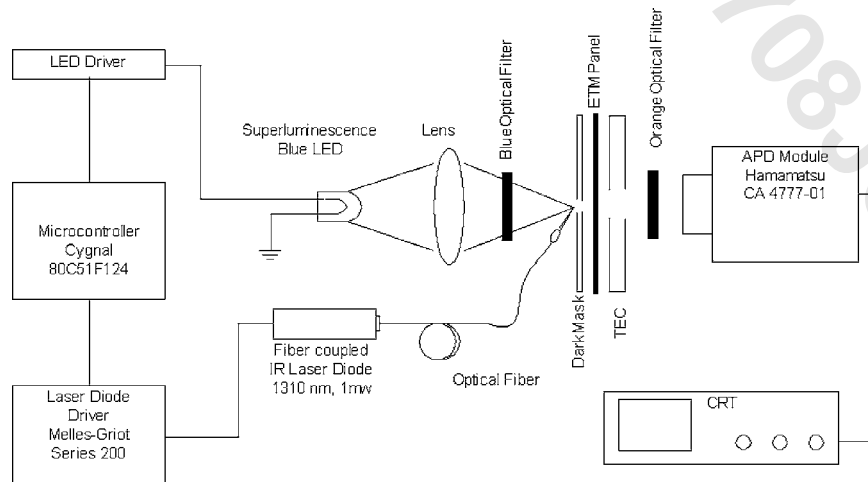
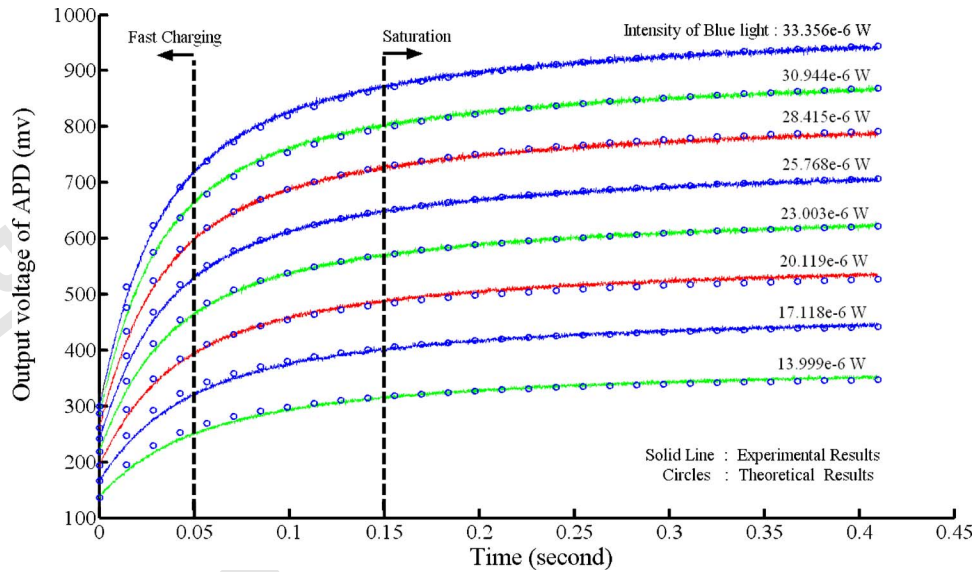


Fig. 2. Schematic of the experimental setup used for investigation of the ETM's dynamics.



Color: Online Fig. 3. (Color online) Charging characteristic curves of the partially erased ETM under blue light illumination. Three points should be considered in the study of these curves: the initial jumps (at  $t=0.0$ ), the relatively linear buildup in the initial moments, and the final saturations. The solid curves are the experimental results, and the circles are the curve-fitting data.

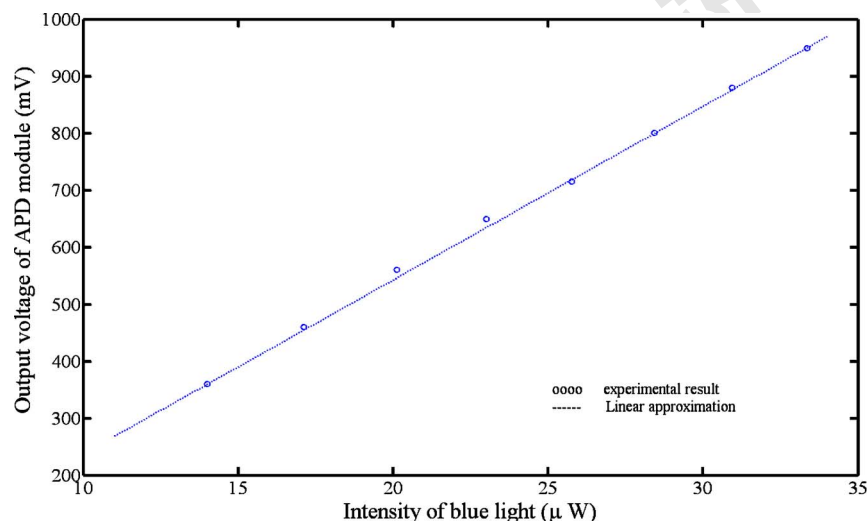
147 The output voltage of the APD module is connected to  
 148 the analog input terminal of the microcontroller's analog  
 149 to-digital converter (ADC). A center-hole thermoelectric  
 150 cooler (TEC) is thermally coupled to the quartz substrate.  
 151 Cooling the ETM decreases the chance of electron-phonon  
 152 interaction and the self-luminescence of the phosphor.  
 153 Also, it has been shown that the orange light emission of  
 154 the ETM increases by decreasing the temperature of the  
 155 material [16]. Therefore, the TEC improves the signal-to-  
 156 noise ratio.

157 In the first experiment, we investigate the charging  
 158 process of the ETM under blue light illumination. At the  
 159 beginning, the blue LED is off when the ETM is exposed  
 160 to the NIR laser, and the APD module measures the in-  
 161 tensity of the orange light emission. When the output  
 162 voltage of the APD reaches a constant predefined value,  
 163 the microcontroller's DAC turns off the NIR laser and

turns on the blue LED with a specified electric current. 164  
 Next, the microcontroller's ADC digitizes and records the 165  
 output voltage of the APD for a fraction of a second. 166

We repeat a similar protocol sequentially with different 167  
 blue light intensities. Figure 3 displays the charging char- 168  
 acteristic curves developed. Three key points should be 169  
 noted in the study of the results obtained: the initial jump 170  
 in the intensity of the emitted orange light at the begin- 171  
 ning of the blue light illumination, its relatively linear be- 172  
 havior during the initial few milliseconds, and the final 173  
 saturation. 174

The existence of different saturation levels can be jus- 175  
 tified by considering that blue photons have sufficient en- 176  
 ergy not only to excite the electrons of the valence band 177  
 and send them to the trap level, but also to detrapp some of 178  
 the trapped electrons. The final saturation represents the 179  
 equilibrium state of these two opposing processes. The 180



Color: Online Fig. 4. (Color online) Saturation levels of the partially erased ETM as a function of the charging blue light intensity and the corresponding linear approximation.



181 level of saturation is a function of the blue light intensity.  
 182 This dependency can be approximated by a linear func-  
 183 tion as shown in Fig. 4. Although the ETM is primarily  
 184 erased to the same density of trapped electrons before all  
 185 the charging periods, each curve has a different initial  
 186 jump. This observation suggests that under blue light il-  
 187 lumination the intensity of orange light luminescence is a  
 188 function of both the trapped-electron density and the in-  
 189 tensity of the incident blue light.

190 The saturation level of the orange light emission is one  
 191 of the ETM's critical parameters in the design of nonlin-  
 192 ear optical devices (as will be described later) and it needs  
 193 to be investigated further. From the charging curves of  
 194 Fig. 3, it is apparent that the saturation level is a function  
 195 of the blue light intensity. However, these curves were de-  
 196 veloped by charging an ETM that was primarily dis-  
 197 charged to a constant predefined trapped-electron density.  
 198 Hence, an unanswered question remains: Does the inten-  
 199 sity of orange luminescence reach the same saturation  
 200 level when the charging process, with constant blue light  
 201 intensity, starts from different trapped-electron densities?

202 To answer this question, a series of experiments was  
 203 performed as follows. First, the precharged ETM is ex-  
 204 posed to an intense NIR light while the APD module mea-  
 205 sures the level of the orange light emission. Next, for a  
 206 fraction of a second, the partially discharged ETM is illu-  
 207 minated by a constant blue light. Simultaneously, the mi-  
 208 crocontroller's ADC digitizes and records the intensity of  
 209 the orange light luminescence. We repeat this experiment  
 210 with a similar protocol, but in each trial, the NIR light is  
 211 turned off at different values of the APD output voltage.  
 212 Thus, the charging process in each trial starts from a dif-  
 213 ferent density of trapped electrons. The curves developed  
 214 in this process are displayed in Fig. 5. The curves of Fig.  
 215 5(b) are similar to the ones illustrated in Fig. 5(a) with  
 216 more emphasis on initial moments. The experimental re-  
 217 sults in Fig. 5(a) show that the final saturation level is in-  
 218 dependent of the initial trapped-electron density. The  
 219 curves of Fig. 5(b) illustrate that the slope of the charging  
 220 curve depends on the initial conditions. The charging  
 221 curves that start from a higher density of the trapped  
 222 electrons have larger slopes compared with the curves

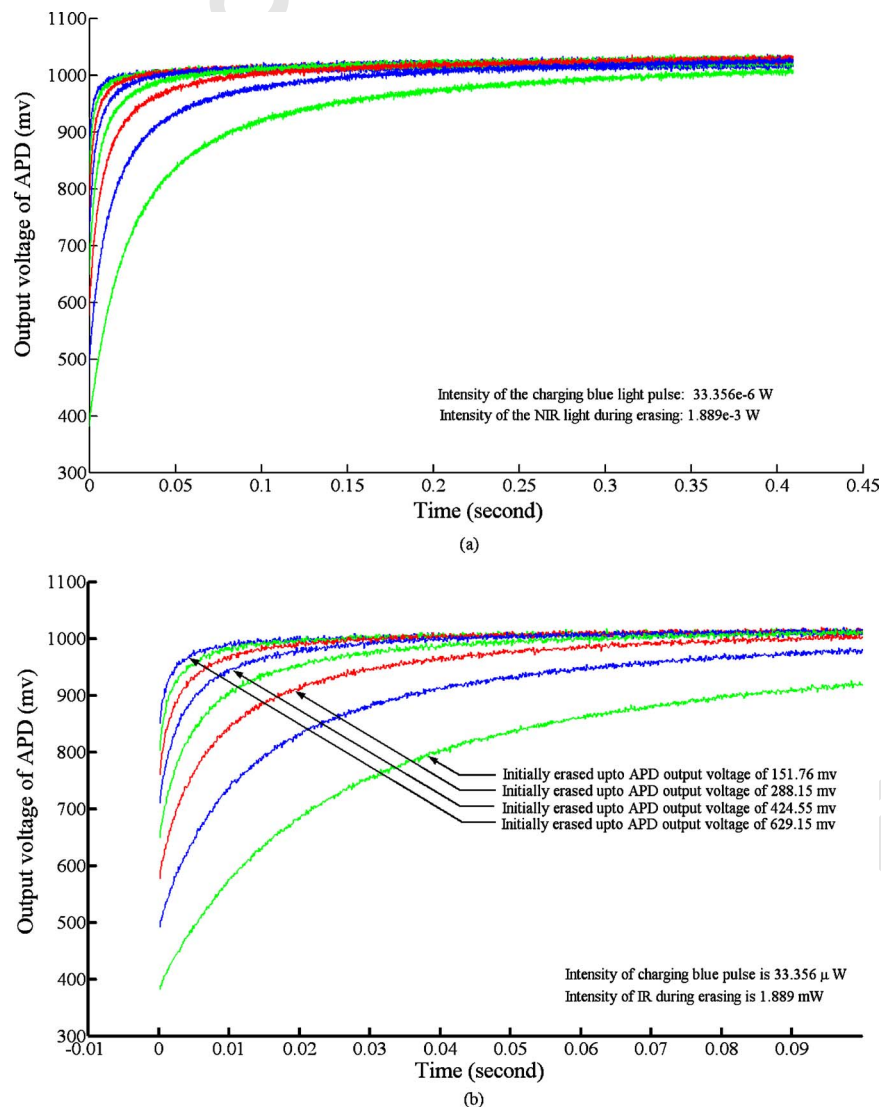
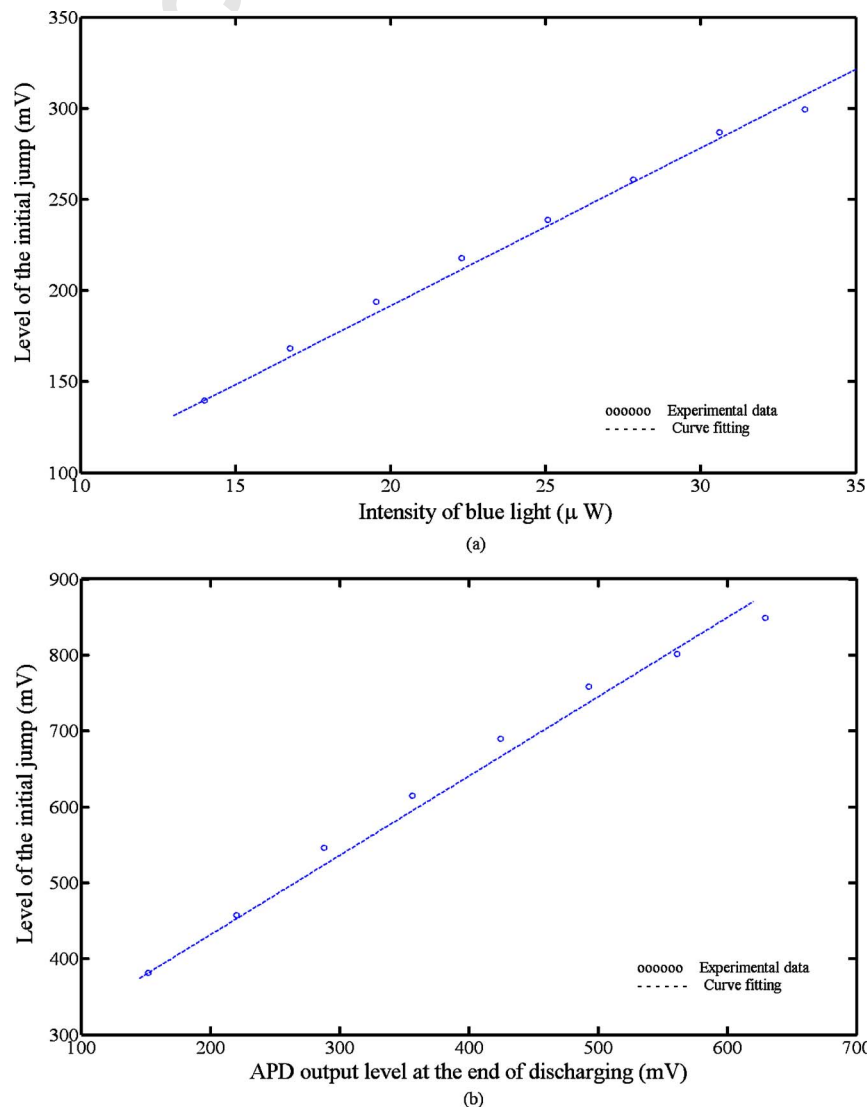


Fig. 5. (Color online) Charging of the partially erased ETM by constant blue light illumination. (a) Despite different initial density of trapped electrons, all the curves merge to the same saturation level. (b) Different initial jumps under constant blue light illumination.

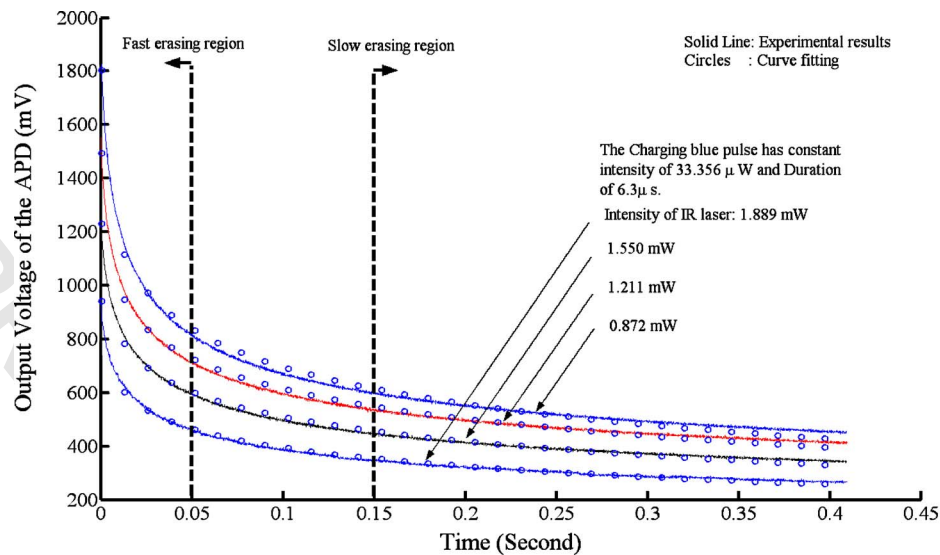
223 starting from a lower trapped-electron density. The ETM  
 224 charges faster when the charging process starts with a  
 225 higher density of trapped electrons. This observation will  
 226 be used later in the design of a nonlinear optical device.  
 227 Figure 6(a) displays the levels of the initial jumps as a  
 228 function of the intensity of the blue light when the initial  
 229 density of the trapped electrons is constant. It is clear  
 230 that the experimental data can be approximated by a lin-  
 231 ear function. The graph of Fig. 6(b) illustrates the levels  
 232 of the initial jumps as a function of the initial trapped-  
 233 electron density, when the intensity of the incident charg-  
 234 ing blue light is constant. Again, the experimental data  
 235 developed can be approximated by a linear function. By  
 236 investigating the data developed from these experiments,  
 237 the relation between the intensity of the orange lumines-  
 238 cence and the intensity of the charging blue light can be  
 239 formulated. The intensity of the orange light emission is a  
 240 linear function of the blue light intensity when the charg-  
 241 ing process starts from equal initial densities of trapped

242 electrons. The intensity of the orange luminescence is also  
 243 a linear function of the density of the trapped electrons  
 244 during the charging process with constant blue light in-  
 245 tensity. Consequently, the intensity of the orange light  
 246 emission during the charging process is proportional to  
 247 the product of the current value of the trapped-electron  
 248 density and the intensity of the blue light.

249 The same experimental setup is used to extract the dis-  
 250 charging curves of ETM. We perform this experiment in  
 251 three sequential steps. First, the ETM is exposed to in-  
 252 tense NIR illumination that detraps almost all the  
 253 trapped electrons. In the second step, the ETM is exposed  
 254 to a pulse of blue light with a constant intensity and du-  
 255 ration. In the third and last step, the ETM panel is illu-  
 256 minated by a constant NIR light while the intensity of the  
 257 emitted orange light is digitized and recorded. Then, the  
 258 same protocol is repeated by changing the intensity of the  
 259 NIR light in the last step of the experiment. The group of  
 260 curves displayed in Fig. 7 represents the results of the



Color: Online Fig. 6. (Color online) (a) Levels of the initial jumps as a function of the intensity of the blue light when the initial density of the trapped electrons is constant. The experimental data can be approximated by a linear function. (b) The levels of the initial jumps as a function of the initial trapped-electron density when the intensity of the incident charging blue light is constant. Again, the experimental data can be approximated by a linear function.

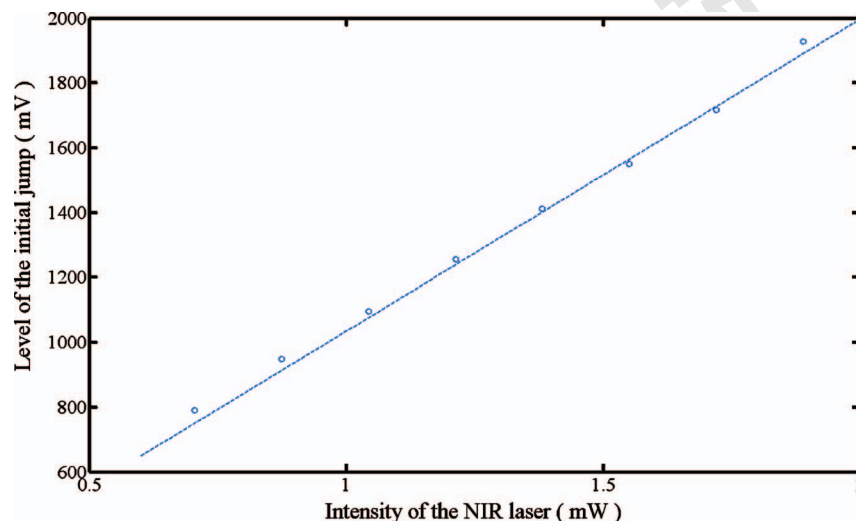


Color: Online Fig. 7. (Color online) Discharging characteristic curves of the ETM. The discharging process has two separable phases. In the first phase, the intensity of the orange light emission drops rapidly after an abrupt jump. During the second phase, the intensity of the orange light emission decreases slowly.

261 discharging experiment. These curves show that the dis-  
 262 charging process has two different phases. During the  
 263 first phase, which occurs at the initial moment, the inten-  
 264 sity of the emitted orange light drops rapidly and the dis-  
 265 charging process is even faster than the exponential func-  
 266 tion. The initial jumps and the slopes of the curves in this  
 267 figure are functions of the initial density of the trapped  
 268 electrons and the intensity of the NIR exposure, the  
 269 higher the initial density of trapped electrons, the steeper  
 270 the discharging process. During the second phase, the or-  
 271 ange light emission decreases slowly and the discharging  
 272 process is slow. Figure 8 displays the levels of the initial  
 273 jumps as a function of the discharging NIR light intensity.  
 274 The experimental results in this graph can be approxi-  
 275 mated by a linear function. Hence, as with the charging  
 276 process, the intensity of the orange light emission during  
 277 discharging is proportional to the product of the intensity

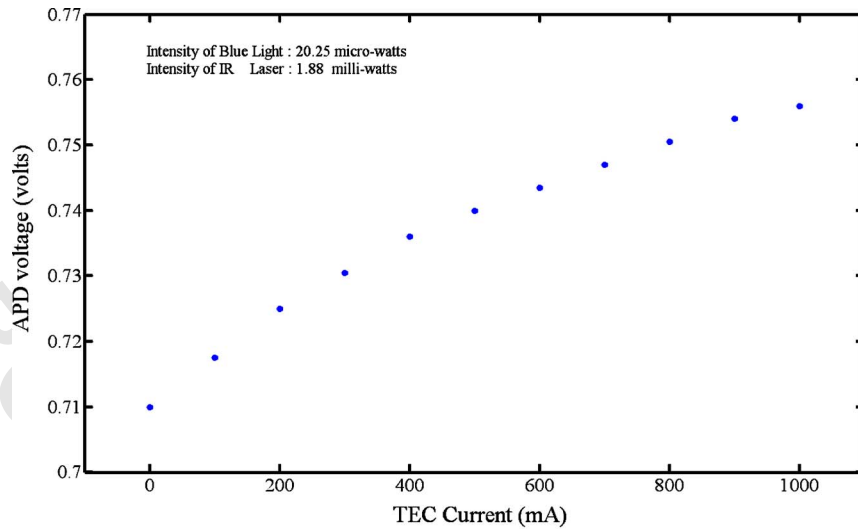
of the NIR light and the existing value of the trapped-  
 electron density.

Figure 9 illustrates the effect of temperature on the in-  
 tensity of the orange light emission. In this experiment,  
 the ETM panel is simultaneously exposed to the blue light  
 and the NIR laser, and the equilibrium-state emission of  
 the ETM is recorded under different TEC currents. This  
 experiment elucidates that increasing the current of the  
 TEC (which is equivalent to reducing the temperature of  
 ETM) increases the intensity of the emitted orange light  
 and improves the corresponding signal-to-noise ratio of  
 the APD module output voltage. In practice, by cooling  
 the ETM, detectors with lower sensitivity that are  
 cheaper and available in array formats can be employed.  
 This could become a critical issue during realization of  
 multipixel systems. The temperature dependence of the  
 photoluminescence in the singly doped ETMs ( $\text{SrS}:\text{Em}^{2+}$ )



Color: Print Fig. 8. Levels of the initial jumps as a function of the discharging NIR light intensity. A linear function can be fitted to the experimental results.





Color: Online Fig. 9. (Color online) Effect of temperature on the intensity of the emitted orange light when the ETM is under simultaneous blue light and NIR light illumination. This curve proves that at lower temperatures, the orange light emission is more intense.

295 and SrS:Sm<sup>3+</sup>) as well as the doubly doped ones (e.g.  
 296 SrS:Em<sup>2+</sup>, Sm<sup>3+</sup>) have been extensively studied [16].

297 **4. MATHEMATICAL MODEL**

298 In this section, the dynamics of the ETM under simulta-  
 299 neous blue light and NIR light illumination is cast in the  
 300 form of a nonlinear differential equation based on the ex-  
 301 perimental results discussed in Section 3.

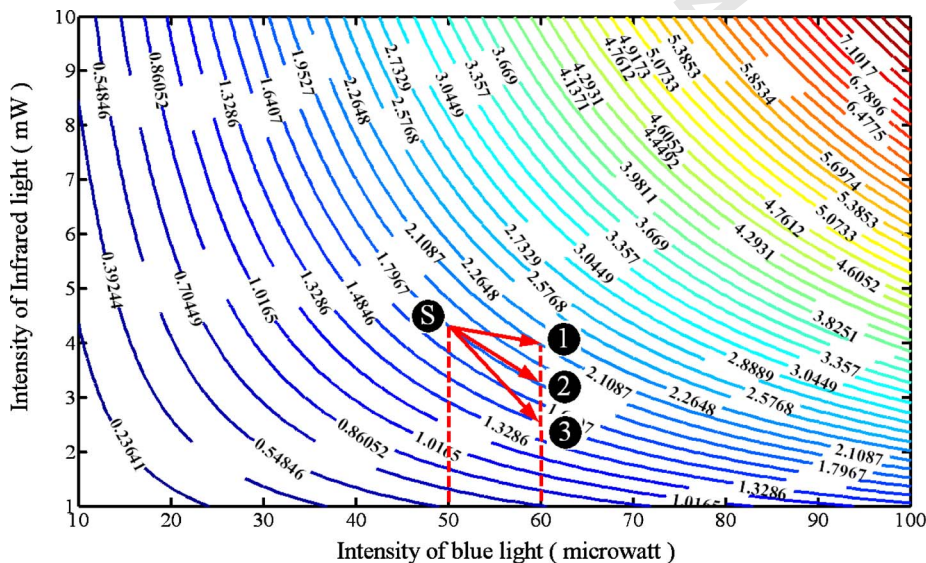
302 Suppose that  $n(t)$  represents the temporal density of  
 303 the trapped electrons as a function of time  $t$ . During the  
 304 charging period when ETM is exposed just to the blue  
 305 light, the density of the trapped electrons  $n(t)$  increases  
 306 monotonically from the initial density of the trapped elec-

trons  $n(0)$  to the saturation density  $n_s$  where  $0 \leq n(t)$  307  
 $\leq n_s$ . By optimal curve fitting [17], the charging process 308  
 can be formulated as 309

$$n(t) = n_s(I_B) - \xi I_B L n \left( \frac{\eta}{t + t_s} + 1 \right). \quad (1) \quad 310$$

The saturation density of the trapped electrons is a func- 311  
 tion of the intensity of the incident blue light  $I_B$ . Follow- 312  
 ing our experimental results (Fig. 4), the dependency of 313  
 the  $n_s$  on the intensity of the charging blue light can be 314  
 approximated by a linear function such as  $n_s(I_B) = \kappa I_B$  315  
 where  $\kappa$  is a real constant. 316

During the discharging period when ETM is exposed to 317  
 the NIR light, the density of the trapped electrons mono- 318



AQ: #7 Fig. 10. (Color online) ESP of electron-trapping material and the unexpected behavior of the ETM luminescence in the equilibrium state.

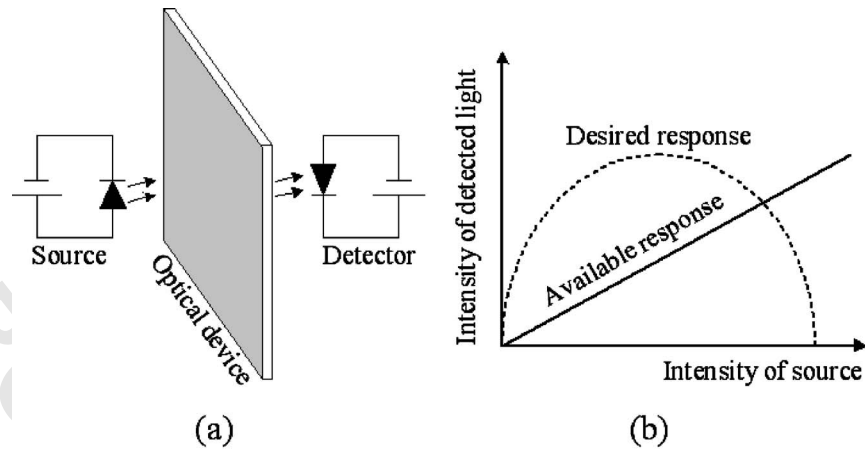
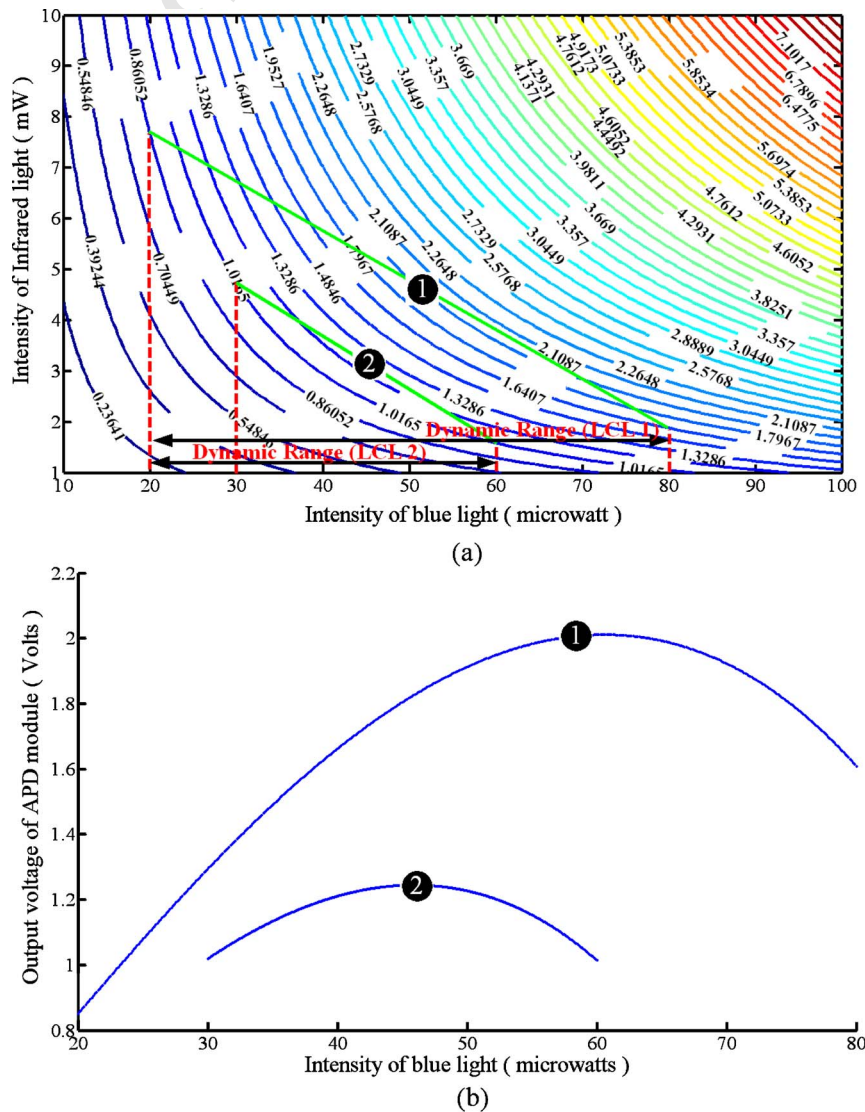


Fig. 11. (a) Optical setup. A light source illuminates the optical device and a detector measures the intensity of the light that passes through the optical device. (b) Available and desired response curves.



**Color:** Fig. 12. (Color online) (a) Two sample LCL and their dynamic ranges along the blue light intensity axis in the ESP of the ETM. Only the intensities of the emitted orange light along the LCLs are accessible when the light sources are linearly coupled. (b) The corresponding nonlinear curves.

319 tonically decreases. As with the charging process, the dis-  
 320 charging process is formulated by optimal curve fitting  
 321 [17] as

$$n(t) = \xi' I_{\text{NIR}} L n \left( \frac{\eta'}{t + t_{s'}} + 1 \right) \quad (2)$$

322  
 323 where  $I_{\text{NIR}}$  is the intensity of the NIR light. In Eqs. (1)  
 324 and (2),  $\xi$  and  $\xi'$  are the ETM wavelength-dependent sen-  
 325 sitivity coefficients to the blue light and the NIR light ex-  
 326 posures. Variables  $\eta$  and  $\eta'$  are the curve fitting param-  
 327 eters, and the initial jumps during the charging and the  
 328 discharging processes are modeled by the variables  $t_s$  and  
 329  $t_{s'}$ , respectively. Obviously,  $t_s$  and  $t_{s'}$  are functions of the  
 330 initial density of the trapped electrons  $n(0)$  and the inten-  
 331 sity of the blue light and NIR exposure. The curve fittings  
 332 of the experimentally derived data during charging and  
 333 discharging processes are displayed in Figs. 3 and 7.

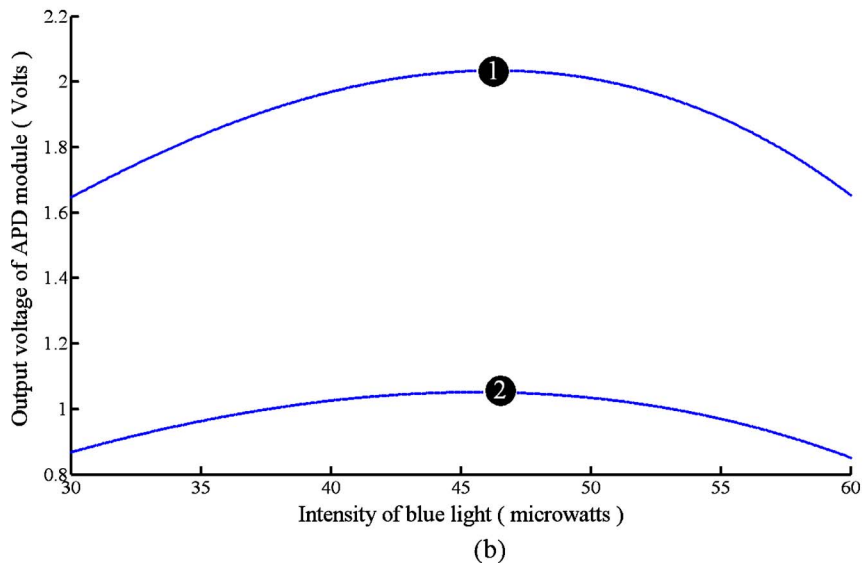
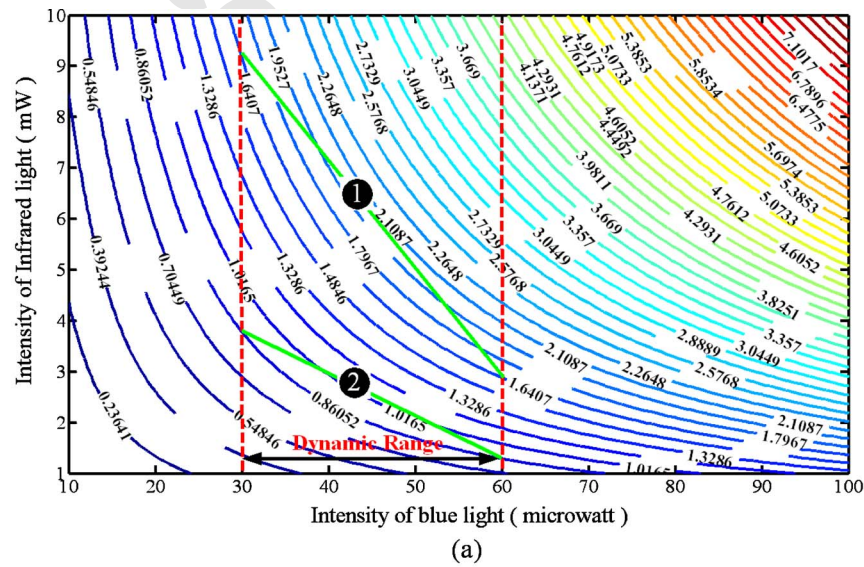
334 In Section 3 it was experimentally proved that  $I_O$ , the  
 335 intensity of the orange light emission under simultaneous  
 336 blue light and NIR illumination, can be expressed as

$$I_O(t) = \alpha n(t) I_B + \beta n(t) I_{\text{NIR}} \quad (3) \quad 337$$

338 where  $\alpha$  and  $\beta$  are the proportionality coefficients for the  
 339 blue light and the NIR light intensities. Usually, we mea-  
 340 sure the intensity of the orange luminescence by a photo-  
 341 detector. The output voltage of this transducer  $V_O$  is pro-  
 342 portional to the illuminating optical intensity:  $V_O \propto I_O$ .  
 343 From Eq. (1), the growth rate of the trapped-electron den-  
 344 sity is

$$\dot{n} = \frac{dn}{dt} = \frac{\xi I_B}{\eta} \frac{\left[ \exp\left(\frac{n_s - n}{\xi I_B}\right) - 1 \right]^2}{\exp\left(\frac{n_s - n}{\xi I_B}\right)} \quad (4) \quad 345$$

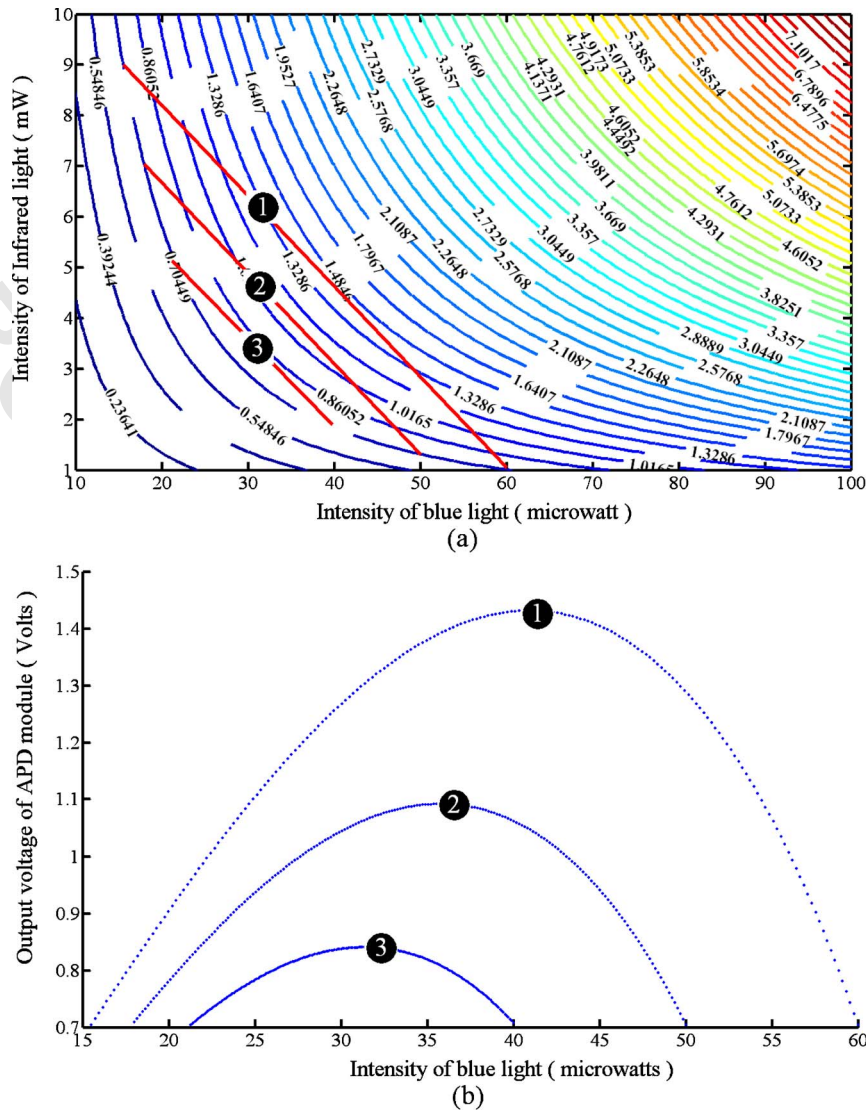
Equation (1) can also be rearranged in the form



Color: Online Fig. 13. (Color online) (a) Two LCLs with the same dynamic range. The termination points of each of these LCLs are located on the same contour. (b) The intensities of the emitted orange light along two LCLs that are depicted in Fig. 14(a).

AQ: #3





Color: Fig. 14. (Color online) (a) Parallel LCLs. All the terminating points are on the same contour. (b) The corresponding nonlinear curves. Online This type of nonlinear curve can be used in the optical generation of one-dimensional maps.

347 
$$\frac{\eta}{t + t_s} = \exp\left(\frac{n_s - n}{\xi I_B}\right) - 1. \quad (5)$$

348 Similarly, using Eq. (2), the reduction rate of the trapped-  
349 electron density during the discharging process is

350 
$$\dot{n} = \frac{dn}{dt} = \frac{\xi' I_{NIR}}{\eta'} \frac{\left[\exp\left(\frac{n}{\xi' I_{NIR}}\right) - 1\right]^2}{\exp\left(\frac{n}{\xi' I_{NIR}}\right)}, \quad (6)$$

351 and by rearranging Eq. (2),

352 
$$\frac{\eta'}{t + t'_s} = \exp\left(\frac{n}{\xi' I_{NIR}}\right) - 1. \quad (7)$$

353 Equations (5) and (7) can be solved for the parameters  $t_s$   
354 and  $t'_s$ :

355 
$$t_s = \frac{\eta}{\exp\left(\frac{n_s - n}{\xi I_B}\right) - 1}, \quad (8)$$

356 
$$t'_s = \frac{\eta'}{\exp\left(\frac{n}{\xi' I_{NIR}}\right) - 1}. \quad (9)$$

357 Now, Eqs. (4) and (6) can also be rewritten in the forms

358 
$$\dot{n} = \frac{4\xi}{\eta} I_B \sinh^2\left(\frac{n_s - n}{2\xi I_B}\right), \quad (10)$$

359 
$$\dot{n} = -\frac{4\xi'}{\eta'} I_{NIR} \sinh^2\left(\frac{n}{2\xi' I_{NIR}}\right). \quad (11)$$

360 The mathematical model for the charging and discharging  
361 processes is expressed in Eqs. (10) and (11). By com-

362 binning these two expressions, we develop the mathemati-  
 363 cal model that governs the dynamics of the ETM under  
 364 simultaneous blue light and NIR illumination:

$$\dot{n} = \frac{4\xi}{\eta} I_B \sinh^2\left(\frac{n_s - n}{2\xi I_B}\right) - \frac{4\xi'}{\eta'} I_{NIR} \sinh^2\left(\frac{n}{2\xi' I_{NIR}}\right). \quad (12)$$

366 Equation (12) provides a complete mathematical model  
 367 for the dynamics of ETM in the form of a nonlinear differ-  
 368 ential equation.

369 Section 5 below is dedicated to the study of the  
 370 equilibrium-state luminescence of ETM, which is the  
 371 equilibrium state of Eq. (12) ( $dn/dt=0$ ):

$$\frac{4\xi}{\eta} I_B \sinh^2\left(\frac{n_s - n^*}{2\xi I_B}\right) = \frac{4\xi'}{\eta'} I_{NIR} \sinh^2\left(\frac{n^*}{2\xi' I_{NIR}}\right), \quad (13)$$

$$I_O^* = \alpha n^* I_B + \beta n^* I_{NIR}. \quad (14)$$

374 In these equations,  $n^*$  and  $I_O^*$  are the trapped-electron

density and the intensity of the orange luminescence in  
 the equilibrium state, respectively. For any specified val-  
 ues of the blue light and NIR light intensities, Eq. (13)  
 can be solved for  $n^*$  by minimizing the error function  
 $erf(n^*)$ :

$$erf(n^*) = \left\| \frac{4\xi}{\eta} I_B \sinh^2\left(\frac{n_s - n^*}{2\xi I_B}\right) - \frac{4\xi'}{\eta'} I_{NIR} \sinh^2\left(\frac{n^*}{2\xi' I_{NIR}}\right) \right\|. \quad (15)$$

In this equation,  $\| \cdot \|$  is the Euclidean norm. If one has the  
 value of  $n^*$ , the intensity of the orange light emission  $I_O^*$  is  
 computable from Eq. (14). By this methodology, one can  
 compute the value of  $I_O^*$  for a wide range of values of  $I_B$   
 and  $I_{NIR}$  and prepare a diagram like the one shown in Fig.  
 10. In this two-dimensional diagram, which is called the  
 equilibrium-state plane (ESP) of the ETM, the contours of  
 constant orange light emission intensity are plotted as a  
 function of the blue light and NIR light intensity for a  
 reasonable range of variables on each axis. The numbers  
 on the contours are the output voltages of the photodetec-

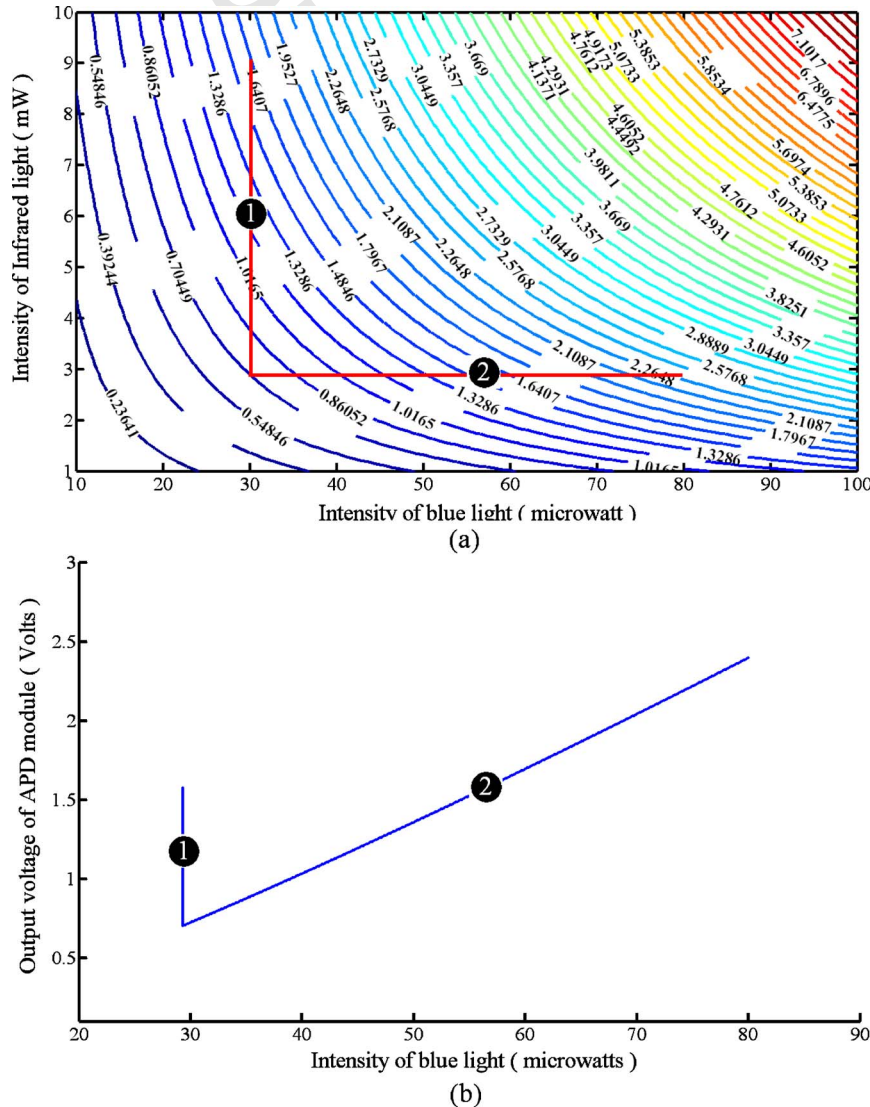
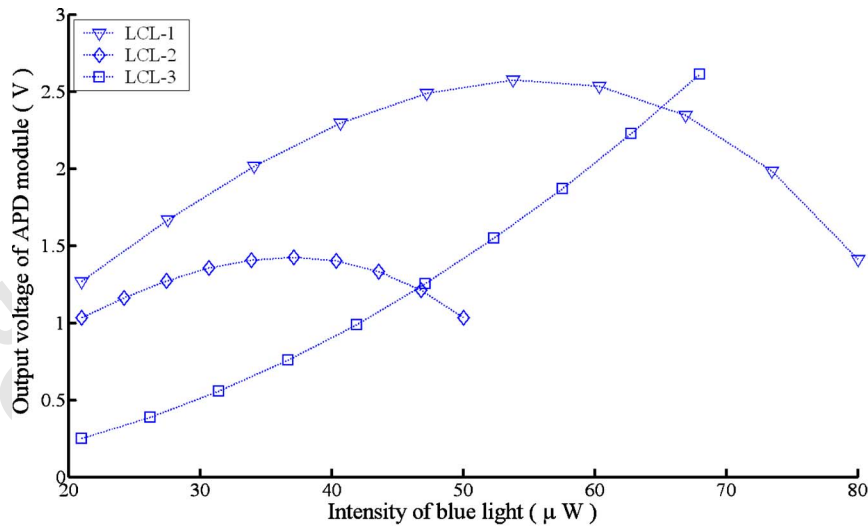


Fig. 15. (Color online) (a) Two LCLs for the generation of the quasi-linear curves. (b) The corresponding quasi-linear curves.

Color:  
 Online





Color: Online Fig. 16. (Color online) Experimental results. Along the first two LCLs, which have negative slopes, (see text) the luminescence of the material changes nonlinearly. Along the third LCL, which has positive slope, the luminescence of the material is quasi-linear.

392 tor that measures the intensity of the orange lumines-  
 393 cence. In Section 5, we will use this diagram as a graphic  
 394 tool to design highly nonlinear optical devices.

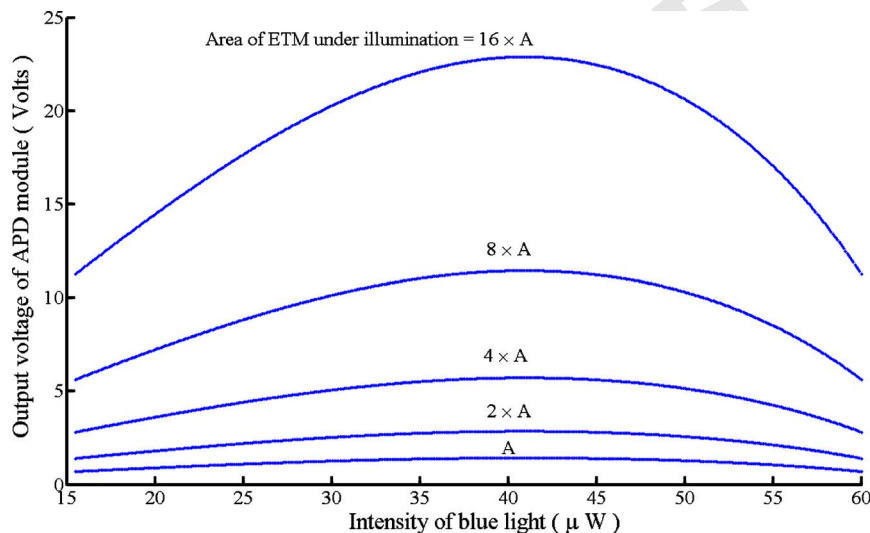
### 395 5. EQUILIBRIUM-STATE LUMINESCENCE

396 The significance of the equilibrium-state luminescence of  
 397 ETM for applications in optical signal processing becomes  
 398 clear by an example. Consider the simple optical arrange-  
 399 ment displayed in Fig. 11(a). A photodetector measures  
 400 the intensity of the light emitted from a light source and  
 401 passed through a passive optical device. Usually, the out-  
 402 put voltage of the photodetector is a linear function of the  
 403 intensity of illumination. However, in many applications  
 404 (e.g., optical realization of one-dimensional maps in non-  
 405 linear dynamics) we require a nonlinear behavior such as  
 406 the desired curve depicted in Fig. 11(b). Here, the inten-  
 407 sity of the detected light increases at first and decreases  
 408 when we pass a maximum point. To our knowledge such  
 409 an optical component is not available. In this section we

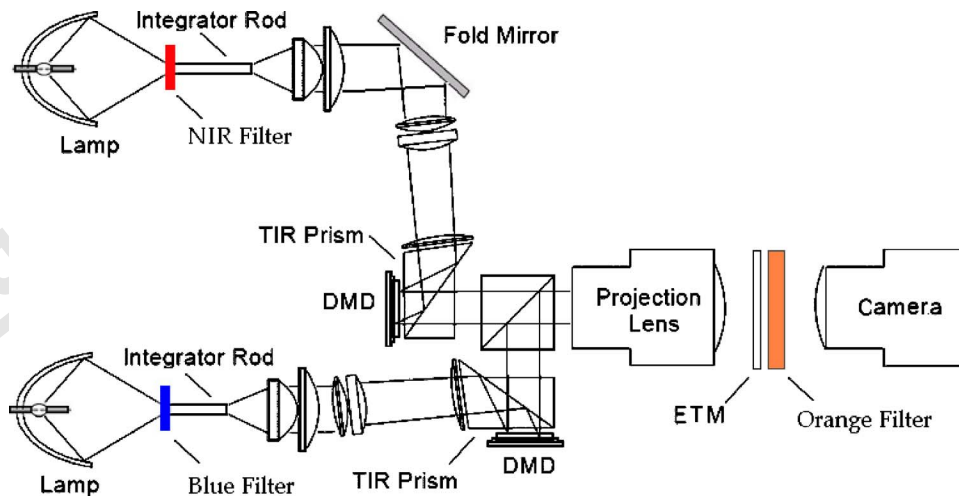
show that the equilibrium-state luminescence of ETM can  
 be controlled to exhibit such a nonlinear behavior. Based  
 on the experimental results and the developed mathemati-  
 cal model, we then present an improved approach for  
 realization and design of such nonlinear optical de-  
 vices.

The behavior of ETM in the equilibrium state can be  
 predicted by using the ESP diagram that was introduced  
 in Section 4. We highlight the subtle utility of the ESP  
 diagram by investigating four sample points, S, 1, 2, and  
 3, in Fig. 10. Point S corresponds to the ETM panel being  
 exposed simultaneously to blue and NIR light with the  
 ETM in the equilibrium state. The intensity of the inci-  
 dent blue light and the NIR exposure are 50 μW and  
 4.35 mW, respectively. The output voltage of the photode-  
 tector that measures the intensity of the orange light lu-  
 minescence is ≈ 1.8 V.

Now, consider the case when the intensity of the blue  
 light is increased from 50 μW to 60 μW, and in three suc-  
 ceeding steps, the intensity of the NIR light is changed to



Color: Online Fig. 17. (Color online) Effect of changing the area of the ETM under illumination. The nonlinear curves are related to the third LCL in Fig. 13(a). The area changes from  $A=3 \text{ mm}^2$  to  $16 \times A$ .



Color: Online Fig. 18. (Color online) Simultaneous illumination of ETM panel with the combined beam of two DMD spatial light modulators. (TIR stands for total internal reflection.)

430 4 mW, 3.2 mW, and 2.6 mW. These new states are the  
 431 points 1, 2, and 3, respectively, in Fig. 10. The output volt-  
 432 ages of the photodetector at these three points are 2.1,  
 433 1.8, and 1.5 V for points 1, 2, and 3, respectively. As a re-  
 434 sult, by increasing the intensity of the blue light from  
 435 point S to points 1, 2, and 3, depending on the intensity of  
 436 the NIR illumination, the intensity of the orange lumines-  
 437 cence increases, remains the same, or decreases, respec-  
 438 tively. Further investigation reveals that the intensity of  
 439 the emitted orange light monotonically increases along  
 440 the line  $S \rightarrow 1$  and decreases along the line  $S \rightarrow 3$ . We have  
 441 recently shown that this kind of behavior can be used to  
 442 model the excitatory and inhibitory responses of the neu-  
 443 rons in optical realization of bio-inspired artificial neural  
 444 networks [18,19].

445 Now consider the special case where the blue and NIR  
 446 light sources are linearly coupled. The linear coupling of  
 447 two light sources can be formulated by the equation

$$448 \quad \mu I_B + \nu I_{\text{NIR}} = \sigma, \quad (16)$$

449 where  $\mu$ ,  $\nu$ , and  $\sigma$  are real numbers. These variables are  
 450 the key parameters in the design of the nonlinear optical  
 451 device. In this paper, the line expressed by Eq. (16) is  
 452 called the linear-coupling line (LCL). In the particular  
 453 case where the light sources are coupled linearly, the op-  
 454 tical device user can change the intensity of only one of  
 455 the light sources. For instance, in this paper, the blue  
 456 light source is the master source, and the NIR light  
 457 source traces the blue light source through Eq. (16). When  
 458 the two light sources are linearly coupled, those orange  
 459 light emission intensities along the corresponding LCL  
 460 only are achievable.

461 Two sample LCLs and their dynamic ranges over the  
 462 horizontal axis are illustrated in Fig. 12(a). The intensity  
 463 of the emitted orange light changes nonlinearly along  
 464 these two lines as shown in Fig. 12(b). A variety of non-  
 465 linear curves are achievable by changing the slope and  
 466 the location of a LCL in the ESP. For instance, the termi-  
 467 nation points of the first LCL in Fig. 12(a) are located on  
 468 the two different constant voltage contours. Therefore,  
 469 the intensities of the emitted orange light are different at

these points. The second LCL has a different slope and  
 dynamic range, and the corresponding nonlinear curve is  
 quite different from the nonlinear curve of the first LCL;  
 however, the termination points are both on the same con-  
 tour. Therefore, the corresponding nonlinear orange light  
 emission curve has equal intensities at the terminating  
 points and the nonlinear curve is more symmetric.

These types of LCLs are suitable for the optical genera-  
 tion of nonlinear one-dimensional maps. Figure 13(a) dis-  
 plays two different LCLs with the same dynamic range.  
 The corresponding nonlinear curves are illustrated in Fig.  
 13(b). In spite of similar dynamic ranges, these LCLs  
 have different slopes and termination points. Hence, the  
 corresponding nonlinear curves are different. A subtle dif-  
 ference between these two nonlinear curves is the speed  
 of computation on these two LCLs. It should be remem-  
 bered that all these curves are achievable in the equilib-  
 rium state of the ETM, which means that each time the  
 intensities of the blue light and the NIR light are set, the  
 user should wait for the equilibrium state to occur. The  
 equilibrium is reached sooner for higher intensities of the  
 blue and NIR light and larger density of the trapped elec-  
 trons. The ETM reaches the equilibrium state faster  
 along the second LCL of Fig. 13(a) than along the first  
 LCL. Meanwhile, the intensity of orange luminescence is  
 higher along the first LCL compared with the second one  
 and the detected signal has a larger signal-to-noise ratio.

Now consider the case depicted in Fig. 14(a). In this fig-  
 ure, three parallel LCLs are shown in the ESP of the  
 ETM. The corresponding orange light emission curves  
 along these LCLs are shown in Fig. 14(b). The termina-  
 tion points of these three LCLs are placed on the same  
 contour that represents the photodetector output voltage  
 of  $\approx 700$  mV. These three LCLs are parallel to each other.  
 Therefore, the parameters  $\mu$  and  $\nu$  in Eq. (16) are fixed,  
 and the parameter  $\sigma$  is the only variable. In nonlinear-  
 dynamic applications,  $\sigma$  can play the role of the bifurca-  
 tion parameter. By normalizing the dynamic ranges of  
 these lines, the developed nonlinear curves will look like  
 the curves that are used in the generation of a one-  
 dimensional map such as the logistic map in [20]. We  
 should mention that the quasi-linear behavior can also be

generated by the equilibrium state of the ETM when the LCLs are chosen appropriately. Figs. 15(a) and 15(b) illustrate two LCLs and the corresponding quasi-linear functions, respectively.

In order to verify the above formulations an experiment was carried out using the optical setup of Fig. 2. We chose the following LCLs and measured the intensity of the orange luminescence in the equilibrium state along each line:

$$\text{LCL-1: } -0.14I_B + I_{\text{NIR}} = 12.0,$$

$$\text{LCL-2: } -0.18I_B + I_{\text{NIR}} = 11.0,$$

$$\text{LCL-3: } +0.05I_B + I_{\text{NIR}} = 0.0.$$

The results are shown in Fig. 16. In all these experiments, the surface of the ETM panel is covered by a dark optical mask with a small aperture. Thus, the area of the ETM under illumination is fixed. On the other hand, one can effectively take advantage of the area as a parameter in the design of the nonlinear optical device. For a constant blue and NIR light illumination, the level of the orange light emission changes linearly as a function of the area of the ETM under illumination. Figure 17 shows the nonlinear curves developed by changing the illuminating area for the third LCL in Fig. 14(a). We can use these curves for the optical production of the one-dimensional maps without any normalization.

One can easily change the area of ETM under illumination by using a spatial light modulator such as the Texas Instruments digital micromirror device (DMD) [21]. A sample optical setup is depicted in Fig. 18. A DMD chip is a two-dimensional array of bistable programmable micromirrors. Two DMD modules in the setup provide the blue light and the NIR illuminations by reflecting the beam of two powerful light sources. By changing the number of mirrors, whose reflections expose the surface of the ETM, the illuminating area can be changed. DMDs are fast enough to adjust the area every few milliseconds, which is shorter than the few hundred milliseconds required for an ETM to reach the equilibrium state.

## 6. CONCLUSION

We have introduced an improved mathematical model that governs the dynamics of ETMs under blue light and near-infrared illumination. The model describes the evolution of an ETM's luminescence during charging, discharging, simultaneous illumination, and in the equilibrium state. This model, which is established based on the experimental results and takes into account some of the previously neglected effects, can improve the applicability of the ETM's unique dynamics, particularly in quantitative applications such as optical signal processing. We have also studied the nonlinear response of ETMs in the equilibrium state. This nonlinear response has potential applications in nonlinear optical signal processing and optical implementation of one-dimensional maps. There are occasions where collective processing in multiple one-dimensional maps needs to be considered. An obvious example of these applications are networks of one-

dimensional maps [22–24]. The parallel computation carried out by such networks can be realized in a thin film of this storage phosphor addressed suitably employing DMD technology. Consequently, our mathematical model would be an important tool for effective use of an ETM's dynamics.

## ACKNOWLEDGMENTS

This research was supported in part by Army Research Office Multidisciplinary University Research Initiative grant prime DAAD 19-01-0603 via Georgia Institute of Technology subcontract E-18-677-64 and in part by Office of Naval Research grant N00014-94-1-0931.

## REFERENCES AND NOTES

- J. Lindmayer, "A new erasable optical memory," *Solid State Technol.* **31**, 135–138 (1988).
- J. Lindmayer, P. Goldsmith, and K. Gross, "Electron-trapping optical technology—memory's next generation," *Comput. Technol. Rev.* **10**, 37–42 (1990).
- S. Jutamuli, G. Stori, J. Lindmayer, and W. Seiderman, "Use of electron trapping materials in optical signal processing. 1: parallel Boolean logic," *Appl. Opt.* **29**, 4806–4811 (1990).
- A. D. McAulay, J. Wang, and C. T. Ma, "Optical dynamic matched filtering with electron trapping devices," in *Real-Time Signal Processing XI*, J. P. Letellier, ed., *Proc. SPIE* **977**, 271–276 (1988).
- S. Jutamuli, G. Stori, J. Lindmayer, and W. Seiderman, "Use of electron trapping materials in optical signal processing. 2: two-dimensional associative memory," *Appl. Opt.* **30**, 2879–2884 (1991).
- S. Jutamuli, G. Stori, J. Lindmayer, and W. Seiderman, "Use of electron trapping materials in optical signal processing. 3: modified Hopfield type neural networks," *Appl. Opt.* **30**, 1786–1790 (1991).
- A. D. McAulay, J. Wang, and C. T. Ma, "Optical orthogonal neural network associative memory with luminescence rebroadcasting devices," in *Proceedings of the IEEE International Conference on Neural Networks* (*Proc. IEEE* 1989) pp. 483–485.
- F. Itoh, K. Kitayama, and Y. Tamura, "Optical outer-product learning in a neural network using optically stimutable phosphor," *Opt. Lett.* **15**, 860–862 (1990).
- S. Jutamulia, G. Storti, J. Lindmayer, and W. Seiderman, "Optical information processing systems and architectures," *Proc. SPIE* **1151**, 83–xx (1990).
- P. Soltani, D. Brower, and G. Storti, "Electron image tubes and image intensifiers," *Proc. SPIE* **1243**, 114–xxx (1990).
- S. Keller, J. Mapes, and G. Cheroff, "Studies on some infrared stimutable phosphors," *Phys. Rev.* **108**, 663–676 (1957).
- Z. Wen and N. Farhat, "Dynamics of electron trapping materials for use in optoelectronic neurocomputing," *Appl. Opt.* **32**, 7251–7265 (1993).
- Z. Wen, N. Farhat, "Electron trapping materials and electron-beam-addressed electron trapping material devices: an improved model," *Appl. Opt.* **34**, 5188–5198 (1995).
- X. Yang, C. Y. Wrigley, and J. Lindmayer, "Three-dimensional optical memory based on transparent electron thin film," *Proc. SPIE* **1773**, 413–422 (1992).
- The electron-trapping material used for this investigation was furnished by the former Quantex Corporation, Rockville, Maryland, USA.
- Z. Hua, L. Salamanca-Riba, M. Wuttig, and P. K. Soltani, "Temperature dependence of photoluminescence in SrS:Eu<sup>2+</sup>,Sm<sup>3+</sup> thin films," *J. Opt. Soc. Am. B* **10**, 1464–1469 (1993).
- S. Boyd and L. Vandenberghe, *Convex Optimization*,

- 636 available online at <http://www.stanford.edu/boyd/cvxbook.html> (Cambridge U. Press, 2004).
- 637
- 638 18. R. Pashaie and N. H. Farhat, "Optical realization of the
- 639 retinal ganglion receptive fields in electron-trapping
- 640 material thin film," Proceedings of 32nd Northeast
- 641 Bioengineering Conference, Easton, Penn., USA (2006).
- AQ: 642 19. R. Pashaie and N. H. Farhat, "Realization of receptive
- #5 643 fields with excitatory and inhibitory responses on the
- 644 equilibrium-state luminescence of electron trapping
- 645 material thin film," Opt. Lett. (to be published).
- 646 20. S. H. Strogatz, *Nonlinear Dynamics and Chaos: With*
- 647 *Applications to Physics, Biology, Chemistry and*
- 648 *Engineering* (Da Capo Press, 1994).
21. D. Dudley, W. M. Duncan, and J. Slaughter, "Emerging 649  
digital micromirror device (DMD) applications," Proc. SPIE 650  
**4985**, 14–25 (2003). 651
22. K. Kaneko, "Overview of coupled map lattices," Chaos **2**, 652  
pp. 279–282 (1992). 653
23. N. H. Farhat, "Corticonics: the way to designing machines 654  
with brain-like intelligence," Proc. SPIE **4109**, 103–109 655  
(2000). 656
24. N. H. Farhat, "Corticonic networks for higher-level 657  
processing," Proc. 2nd IASTED, Feb. 23–25 (2004), pp. 658  
256–262. 659
- AQ: #6

AUTHOR QUERIES — 545708JOB

- #1 Au: Claims of “new” deleted for legal reasons.
- #2 Au: Please define “lp” in “lp/mm”
- #3 Au: Check math in Eq. (4). Are parens and brackets as meant? Also in following equations?
- #4 Au: Please provide ending page number Refs. 9 and 10
- #5 Au: Please provide full dates of conference OR name of publisher of proceedings for Ref. 18.
- #6 Au: Ref. 24: Please provide full name of conference; spell out IASTED; give year of conf. and location.
- #7 Au: Fig. 10 caption: Is “unexpected” as meant?

PROOF COPY [78556] 545708JOB